International Journal Evolving Sustainable and Renewable Energy Solutions ISSN: 3068-9325

PRIME OPEN ACCESS

Volume 1, Issue 2

Research Article

Date of Submission: 29 Sep, 2025
Date of Acceptance: 19 Oct, 2025
Date of Publication: 04 Nov, 2025

Design and Fabrication of a Wet-type Milling Machine and Investigation of Sintering Temperature Effect on Electro-mechanical Properties of $La_{1-x}Zr_xCo_{1-y}Mn_yO_3$ Perovskite Oxide for IT-SOFC Cathode

Abdullah Al Fuad[3*], Md Abu Daud[1] and Robel Ahmed[2]

[1]Bangladesh Army University of Science and Technology (BAUST), Department of Mechanical Engineering, Saidpur Cantonment, Bangladesh

[2]Rajshahi University of Engineering & Technology (RUET), Bangladesh

[3]National Institute of Textile Engineering and Research, Nayarhat, Savar, Bangladesh

***Corresponding Author:** Abdullah Al Fuad, National Institute of Textile Engineering and Research, Nayarhat, Savar, Bangladesh.

Citation: Fuad, A. A., Daud, M. A., Ahmed, R. (2025). Design and Fabrication of a Wet-type Milling Machine and Investigation of Sintering Temperature Effect on Electro-mechanical Properties of La1–xZrxCo1–yMnyO3 Perovskite Oxide for IT-SOFC Cathode. *Int J Evol Sus Renew Energy Sol, 1*(2), 01-13.

Abstract

The work entails the design and fabrication of a wet type ball milling machine to powder mill. The process of electricity production using solid oxide fuel cells (SOFC) relies on electrochemical oxidation of fuel and research is aimed at improving the performance of SOFC cathodes based on doping lanthanum cobaltate. This study involves adding zirconia (ZrO_2) to a lanthanum cobalt oxide perovskite composite and then assessing its effect on the physical, mechanical, and electrical properties of a composite. In this paper, effect of sintering temperature is investigated by varying different wt.% of ZrO_2 and MnO_2 was changed according to the compound requirement for every sample prepared by the solid-state reaction. The final sintered samples were then undergone through characterization tests in terms of density, Diametral Tensile Strength (DTS) and compressive strength and so on. From the result, it is shown that composite with 5 wt.% of ZrO_2 yields best result.

Keywords: Milling Machine, IT-SOFC, Sintering, Doping

Introduction

Ball mill is a horizontal rotary type of machine, outer gear, two fixed positions and lattice type of ball mill. Feed the device into the mixture using the air evenly into the mill screw shaft first warehouse, and there are ladder liners or corrugated liners, concept according to different specifications steel balls are installed in the cylinder, conveyed the material ball into the action must produce centrifugal force After the fall height, the material and abrasive is anything, produce the severe impact [1].

A fuel cell is an energy-conversion machine which does not intermediate step of direct-combustion since it harnesses the chemical energy of a gaseous fuel and converts it directly into electrical energy and heat. Fuel cells tend to have an extremely high efficiency compared with conventional thermomechanical converters. They work much like batteries: electrochemical oxidation and reduction occurs at electrodes in an ion-conducting electrolyte, where the reactant pairing is a gas of a fuel (e.g., hydrogen) and oxidant (air) oxygen). As opposed to a battery a fuel cell never runs down, nor does it need to be recharged; it will continue to an indefinite future as long as the electrodes are supplied with fuel and oxidant; and the extent of its impact on the environment does not matter. On the table 1 below, the kinds and their

operating temperature and efficiency of fuel cells are given.

Types of Fuel Cells	Operating Temp °C	Efficiency
Alkaline (AFC)	50-200°C	50-55%
Direct Methanol (DMFC)	60-200°C	40-55%
Phosphoric Acid (PAFC)	160-210°C	40-50%
Sulfuric Acid (SAFC)	80-90°C	40-50%
Proton Exchange Membrane (PMFC)	50-80°C	40-50%
Molten Carbonate (MCFC)	630-650°C	50-60%
Solid Oxide (SOFC)	600-1000°C	45-60%
Protonic Ceramic (PCFC)	600-700°C	45-60%

Table 1: Technical Characteristics of Different Fuel Cells [2,3]

Fuel cells are commonly classified by the electrolyte chemistry—the ionic conductor between the anode and cathode—as shown in Table 1. The first five variants operate at low to moderate temperatures (≈50–310 °C) and typically exhibit relatively modest electrical conversion efficiencies: about 40–50% when using readily available fuels such as methanol and other hydrocarbons, and around 50% on pure hydrogen. In contrast, the remaining three types run at high temperatures (≈600–1000 °C), can utilize methane directly in the cell, and show inherently higher generation efficiencies—approximately 45–60% on typical fuels like natural gas, increasing to about 90% when waste heat is recovered. [4]

Wet type ball milling machine

Ball mill is one of the important grinding machines that are utilised in many industries such as cement, silicate and ceramics. It is cylindrical in body structure and spherical in the grinding mediums. It can be applied in wet and dry grinding, where wet grinding has commonly an added classifier and dry grinding has an added suction and separation mechanism. Wet grinding is common and needs either water or anhydrous ethanol, and has better performance and greater efficiency [5].

Benefits

- Wet grinding is efficient. It is less power intensive and its production capacities are high compared to the one caused by dry grinding.
- Flowing of the material is convenient. One will be able to clean its fine particle with water to prevent an over-grind with time.
- The wet ball mill is characterised by few noises and less environmental pollution.
- As the transportation device is simple, and not as many auxiliary facilities are required, the investment is roughly 5 %-10 % lowest compared to that of a dry ball mill.
- The size of grinding however is smooth and refined. The wet ball mill not only grinds agglomerate into smaller particles, but also binds the lean material and the plastic material.

Difficulty

- The wet mill balls have high consumption.
- It gets expensive through the dehydration and drying process.

Solid oxide fuel cell (SOFC)

SOFCs indicate the high-temperature fuel cell technology that offers potential industrial and electricity-generating stations. They permit internally reforming at 600-1000 o C, encourage electrocatalysis and result in high quality byproduct heat to be co-generated. The efficiencies are capable of up to 70 percent with another 20 percent of heat recovery. The most suitable industry in which to utilize SOFCs is the utility sector because of the delay in attaining the ready to operate temperatures.

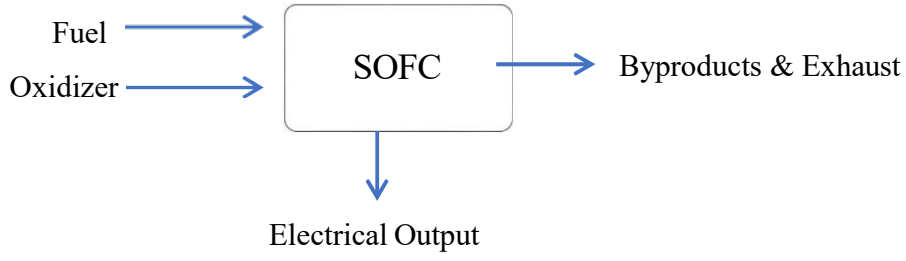

Figure 1: Block Diagram of Electrical Power Generation by SOFC

Solid Oxide Fuel Cells (SOFCs) are unique due to their all-solid-state materials, high temperature capability, and no fundamental configuration restrictions, offering advantages over conventional energy conversion devices.

- The most efficient (in terms of fuel input: electricity output) fuel cell electricity generators under development worldwide are SOFCs.
- The SOFCs allow flexibility in the fuel to be used eg; natural gas - carbon based fuels.
- The SOFC technology would be most ideally applied in the distributed generation (ie, stationary power) sector since high conversion efficiency offers the best gain in the market scenario where the cost of fuel is at a premium (long fuel delivery networks to customer sites).
- The solid-state and modular SOFCs lack any moving parts and so should be rather quiet to be located inside the building.
- High quality heat byproduct generated by SOFCs due to high operating temperature can be utilized in combined cycle, or co-generation applications.
- SOFCs lack electrolyte issues, (e.g. liquid electrolytes, which are corrosive and cumbersome), etc.
- SOFCs exhibit ultra-low emissions by removing the risk of carbon monoxide in the exhaust gases, where carbon monoxide generated is oxidised in the high-operating-temperature environment to carbon dioxide.
- SOFCs have the potential of a long-life span of over 40000/80000 hours.

Construction of SOFC

The typical properties of SOFCs are that their cell components comprise all-solid-state, and operating temperature is 50010008C with a potential system size of 1 kW to 10 MW [6]. In the solid oxide fuel cell (SOFC), a solid electrolyte is utilized and supports two electrodes namely anode and cathode. It is normally fueled by hydrogen, and also SOFCs can work successfully on pure hydrogen. The electrodes also help to introduce reactions between the reactants (fuel and oxygen) without being consumed, at the interfaces of the electrode and the electrolyte. An SOFC uses a dense ceramic-electrolyte typically zirconia, which supports an oxygen-ion gradient; oxygen ions diffuse into the electrolyte and react with the fuel at the anode where electrons are released to external circuit. The overall result is heating and producing electric power; in the case of hydrogen as fuel, water is the only by-product of a reaction (see Figure 2).

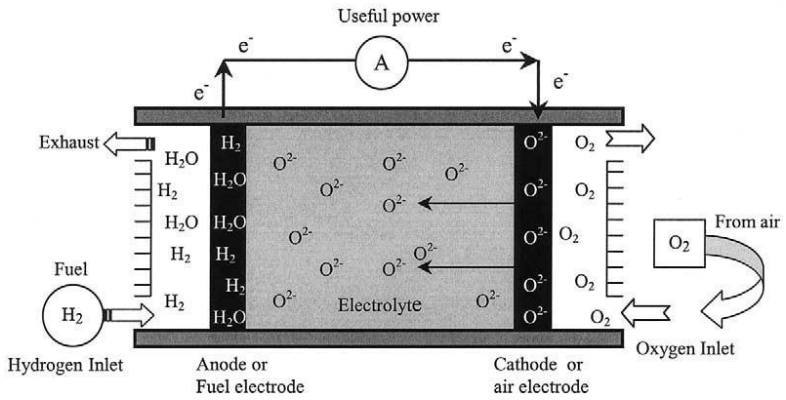

Figure 2: Concept Diagram of SOFC Based on Oxygen-ion Conductors [2]

Reactions in anode:
$H_2 \rightarrow 2H^+ + 2e^-$ (for hydrogen fuel)
$CH_4 + 2H_2O \rightarrow 4H_2 + CO_2 + 8e^-$ (for biogas)
$C_2H_5OH + 3H_2O \rightarrow 2CO_2 + 12H^+ + 12e^-$ (for ethanol) Reactions in cathode:
$O_2 + 4e^- \rightarrow 2O^{2-}$

SOFCs operate at high temperatures, making electrode-supported cells the best choice for reduced temperature applications. Researchers are developing materials and ceramic structures to reduce cell resistance and power density. In the event that the weight, volume, and manufacturing costs are decreased further, and that the target cost of about USD 1000 per kilowatt is attained, the SOFC technology may also prove to be an alternative in generating power on small scales like household power generation. [7]. However, reduction in sintering temperature as well as improving density, hardness, fracture toughness of existing electrolyte materials are also major topics of interest.

Literature Review

A. Calka and A. P. Radlinski: Moreover, the mechanically alloying method, which is used to create composite metallic powders, has been in existence more than two decades. Invention An original ball mill device the pattern of the movement of the balls within the I is controlled by an outer magnetic field [8]. Examples of uses of this ball mill in synthesis of Ni-Zr alloys, high melting point intermetallic, Mg-Zn alloys and aluminum-based alloys are provided. Specifically, the solid- state reaction that takes place in the grinding process can lead to another course when different modes of operation are taken. Vladimir V. Lomakin, Sergey I. Khanin, Natalia P. Putivtseva: Through the use of the methodology, the BEM ball mill was chosen based on the stated requirements of the enterprise [9]. At the initial stage, the number of variants that needed to be considered was reduced to 5 as compared to 8 with the consideration of the

discussed approach. At the 2 nd stage the decision maker selected the most favorable to the enterprise kind as per technical and economic indicators.

Jian Tang a, *, Li-jie Zhao[a,c]: Mill load estimation in real-time is critical towards achieving increased throughput and mill energy efficiency during a grinding process [10]. In this regard, characterizations of the shell vibrations were carried out under various regimes: dry grinding, wet grinding, and water grinding by conducting a sequence of tests. PSD of the vibration signals were studied in a systematic way. Laboratory-scale ball mill signals were collected through an accelerometer fixed at the centre of the mill shell. The transformed data upon sampling were converted to FFT, and pre-processed to estimate these connections between sub band amplitude of PSD and mill-load (ML) descriptors. Lastly, a connection between characteristic frequency bands and ML parameters was specified by a Genetic Algorithm- Partial Least Squares (GA-PLS) modeling approach.

D.W. Fuerstenau a, *, A.-Z.M. Abouzeid [b]: A technical definition of the comminution efficiency depends on a selected measure of machine output divided by the energy input [11]. The controversy remains because the basis of measurement of the output energy is usually not mentioned. Practically both recently developed surface-based efficiency and energy-based numbers have been employed to measure efficiency. Reports on the review of quartz comminution state that depending on the method used, only a percentage of the energy introduced is visible as new surface energy whereby the percentage varies between 0.1 to 1.0. Assuming the energy needed to break new surface by single-particle breakage as the standard, the practical efficiency of ball milling of quartz and soda-lime glass is about 15%. Using a different framing, whereby efficiency is defined as the power required to give a given parameter of the size distribution, dry ball milling of these materials has been encountered to have efficiencies in the vicinity of 25%.

Feliu Maseras, Bruna S. Pladevall: As an emerging field, the means of greener synthesis through the use of mechanical force is in a state of rapid development, the central reaction pathways of which are far less clear even with increasing attention [12]. Mechanochemical routes Mechanochemical protocols are defined by the influence of mechanical energy (milling, grinding, compression) in chemical reaction, and generally occur in neat systems or on catalytic levels of liquid additives (liquid-assisted grinding). This paper shows that conventional computational methods, density functional theory + continuum solvation and microkinetic modelling can be used to probe mechanically activated edge cases. Two exemplary systems are discussed: a DielsAlder cascade (which is a pericyclic reaction with a concerted cyclic transition state at the singlet surface) and the making of sulfonylguanidines. The energetics and rate trends are calculated and are consistent with reported experimental work. The computational workflow is mostly routine, but the accuracy of the model depends sensitively on assumptions regarding intracellular and extracellular concentration and of the effective dielectric environment. Collectively, the findings show that ball-milling leads to rapid reaction rates in these reactions, but does not significantly change elementary reaction mechanisms as compared to solution-phase chemistry.
Today, this worldwide R&D trend is to drop the operating temperature of the solid oxide fuel cells (SOFC) to pave the way towards their wide commercialization. Over several decades, enormous works in SOFC domain have been dedicated to the cathode material development because the

inherent temperature-dependence nature of oxygen reduction reaction in cathode presents a conflict between lower operating temperature and the outstanding cell performance. Perovskite compounds of the type ABO3 (where A is alkaline-earth or rare-earth metal cations and B is transition-metal cations) have attracted high interest because of the structural and compositional versatility, high activity in oxygen reduction reaction, good accessibility and environmental compatibility as a type of typical cathode materials in batteries [13].

Materials

High-purity oxide powders—Co_2O_3, MnO_2, La_2O_3, and ZrO_2—were employed as starting materials. All reagents were procured from Sisco Research Laboratories (SRL), India, and used as received. The reported specifications were: ZrO_2, 99% purity with a nominal particle size of 100– 200 nm; MnO_2, 99% purity with 50–100 nm particles; and Co_2O_3, 99% purity with a particle size of ~10 μm. (No additional size specification was provided for La_2O_3.)

Experimental Procedure

The ball mill is a rotating system consisting of a jar with a diameter and length. The powder and ethanol are rotated through transmission machinery, with silicon balls assisting in mixing the powder. The jar is driven by centripetal force, with big balls at the top and small ones at the bottom. Silicon balls were chosen due to their anti-corrosion properties. The wearing away happens by impact, by friction and by abrasion. There had to be a firm stance to boost the system and mild steel was used to make shafts. The rotational movement or linear motion was attained through the installation of bearings to minimize the friction as well as handling stress.

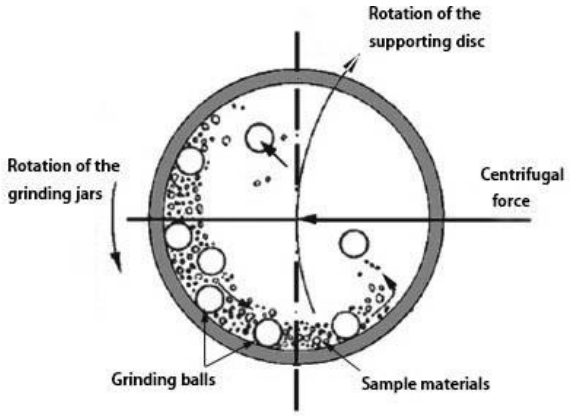

Figure 3: Milling Process of Ball Mill

They prepared four composites pellet batches that are listed in Table 2 and which correspond to various percentages of the raw materials. In the sample preparation, ZrO_2 was retained in the 5 wt%, 10 wt% and 15 wt%. concentration whereas, MnO2 was fixed at 30 wt% and 20 wt%. after which the remaining weight percentages in the sample were made up by the other two raw

materials in the total weight of each sample which was 40gm. The weight was measured with the help of ANDGULF analytical balance (Division: 0.01gm) during the sample preparation.

Fabricated Composites	wt% of ZrO_2	wt% of MnO_2
5LZCM	5	30
10LZCM	10	30
15LZCM	15	30
20LZCM	20	30

Table 2: Compositions of Constituents in the Fabricated Composite

Background The samples used a traditional solid-state synthesis pathway, one approach to making polycrystalline materials through solid sources. Figure 3 shows the fabrication process flow.

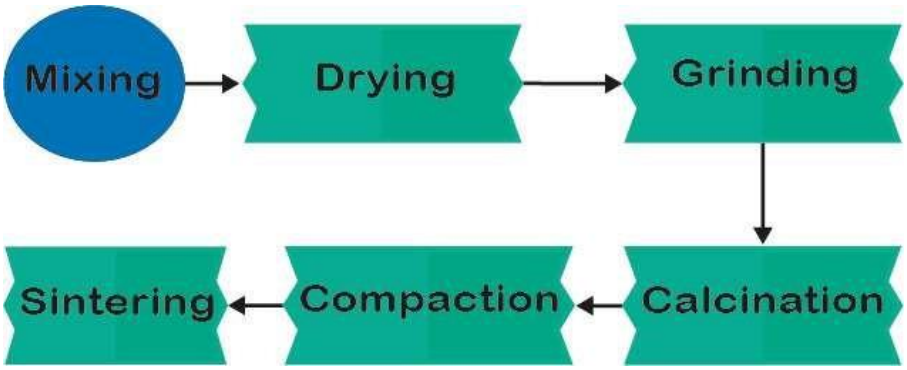

Figure 3: Different Steps of the Fabrication Process

Powders were weighed according to the target composition, and all mixing tools were thoroughly cleaned with detergent, rinsed with distilled water, and finally washed with ethanol. The batch was then wet–ball-milled in a pot mill (Model G91) at 100 rpm for 20 h, using yttria-stabilized zirconia (YSZ) balls as the grinding media and ethanol as the milling solvent. The slurry was dried in a laboratory oven (Jisico, VARO/8P) at 100 °C for 24 h to remove ethanol. The resulting dry cake was gently deagglomerated by hand grinding with a mortar and pestle to obtain a uniform fine powder.

The calcination i.e. purging process took 90 minutes, after which furnace retained a heating rate of 5C/min at 1000 o C. The powder compaction before calcination was eliminated and instead it was performed in order to minimize the impurities and get a good compaction of the powders to form the green bodies.

Pellets ("green bodies") were formed by uniaxially pressing 1.5 g of the composite powder in a pellet press (Retsch, PP25) at 250 MPa for 3 min. Subsequent sintering was performed in a laboratory furnace (Nabertherm, Germany; rated maximum temperature 1600 °C). To obtain the

samples, the heating rate was maintained at 5oC/min temperature was raised to 1200oC in 250 minutes and high

temperature maintenance of 1200oC was maintained in 240 minutes and furnace cooling rate of 420 minutes was done. Sintering gave the intended final composites (Figure 4).

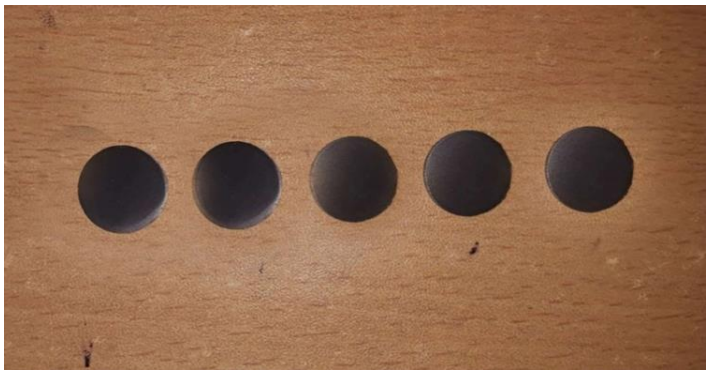

Figure 4: Fabricated Composites

Characterization

Bulk density and open porosity were determined by the Archimedes method. Diametral tensile strength (DTS) was evaluated using a servo-hydraulic universal testing machine (Shenzhen Wance, HUT-106). Vickers microhardness was measured with a Struers DK-2 tester in accordance with ASTM E384, applying loads within 1–1000 gf. Electrical conductivity was obtained from resistance measurements using a custom fixture. The coefficient of thermal expansion (CTE) was recorded with a purpose-built dilatometry setup employing inductive heating. Microstructural features of the sintered surfaces were examined by scanning electron microscopy (TESCAN VEGA COMPACT, Czech Republic), and elemental composition was assessed by EDX using TESCAN ESSENC

Crystalline phases in the sintered pellets were characterized by powder X-ray diffraction using a PANalytical EMP 3 diffractometer (Netherlands) equipped with a Cu source (Cu $K\alpha_1$, λ = 1.54060 Å). Diffraction patterns were analyzed by Rietveld refinement in HighScore Plus to extract phase composition and lattice parameters. Nano Observer, CSI, France was used to perform atomic force microscopy (AFM) studies. The images were analyzed with the help of Gwyddion 2.65 SPM (AFM) Software.

Result and Discussion

Coefficient of Thermal Expansion (CTE)

The effect of ZrO_2 addition on the thermal expansion coefficient is shown in Figure 5 and 6 where the sintering temperature of composites was 1200°C and the ZrO_2 content varied from 0.05 to 0.20 (mole fraction) as A site substitution and MnO_2 content kept at 0.3 (mole fraction) as B site substitution. The figure shows that CTE decreases with the addition of ZrO_2. The minimum CTE of the composite was obtained at 0.15 (Mole Fraction) of ZrO_2 but further addition of ZrO_2, increased the CTE of the composites. The CTE decreased since the nanoparticles of ZrO_2, filled the pores of composites. The grain size of ZrO_2 is smaller than the La2O3Thus increasing the CTE.

As observed by Kim et al., $LnBaCo_2O_{5+\delta}$ (Ln=La, Nd, Sm, Gd and Y) oxides show a decrease in the oxygen content, CTE decreasing size of Ln3+ ions from Ln=La to Y in the system [14]. Cubic double perovskite oxide, $LaSrMnCoO_{5+\delta}$ as investigated by Zhou et al. [15] has an average CTE of 15.8 × 10^{-6} K^{-1} when studied in the temperature range of 30-1000. CTE of $La_{1-x}Sr_xCoFeO_3$ is observed by Y Teraoka and P Huang is 14.8 – 20.1 × 10^{-6} [16-17].

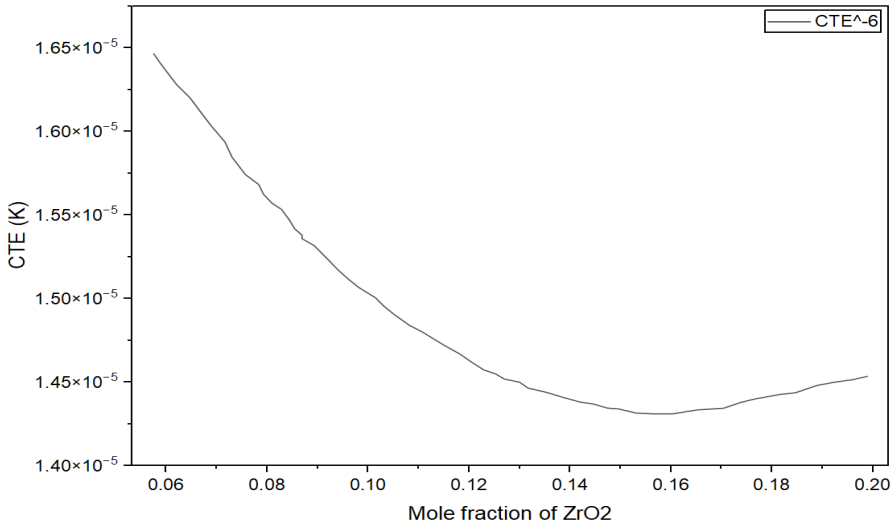

Figure 5: Effect of ZrO_2 Addition on CTE

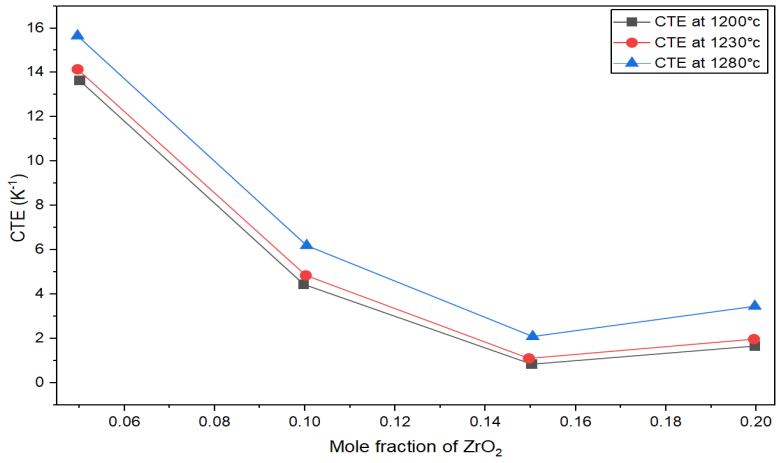

Figure 6: Sintering Temperature on CTE

Electrical Conductivity (σ)

Figures 7-8 present the electronic conductivity of composites sintered at 1300 °C as a function of ZrO_2 addition, varied from 0.05 to 0.20 in mole fraction on the nominal A site, while the B-site MnO_2 content was held constant at 0.30. Conductivity increases monotonically with ZrO_2 content and also rises with temperature. The composition-driven gain can be rationalized by (i) microstructural densification—ZrO_2 nanoparticles (smaller than La_2O_3) help fill residual porosity and improve intergranular contact—and (ii) defect-chemistry effects: aliovalent Zr^{4+} substituting for La^{3+} necessitates charge compensation, elevating the average B-site oxidation state ($Mn^{3+} \rightarrow Mn^{4+}$) and/or adjusting oxygen nonstoichiometry. Both pathways increase the concentration of hole carriers and available hopping sites, thereby enhancing electronic transport. The positive temperature dependence is consistent with thermally activated small-polaron hopping and the activation of intrinsic defects [18]. On the other hand, Manganese-containing perovskites mostly perform electronic compensation which produce an important defect reaction which is charge dis-proportionating reaction by which Mn3+partially disproportionate into Mn2+and Mn4+leading to good electronic conductivity even at lower temperature. When analyzing the electrical conductance using the Arrhenius plot log(σ) versus 1, linear behavior means that the T electronic conductivity is because of the small polaron-hopping mechanism which occurs in the perovskite along the transition metal–oxygen–transition metal chains [19]. Similar results were shown by Kumar et. al [20] where electronic conductivity reached ~700 S/cm (x=0.05, y =0.05) indicating the metallic nature of the samples at high temperatures.

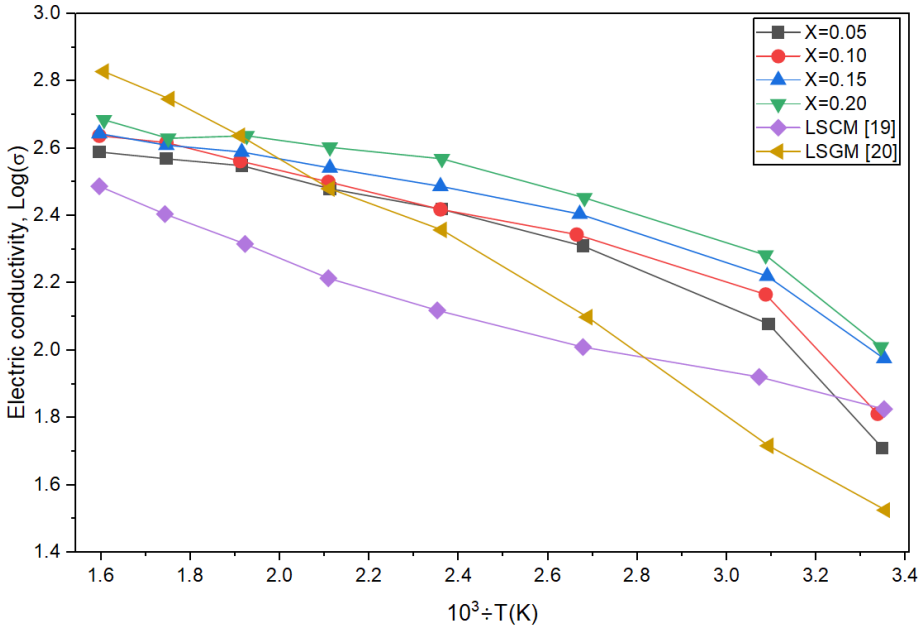

Figure 7: Effect of ZrO_2 Addition on Electronic Conductivity and Comparison with LSCM and LSGM

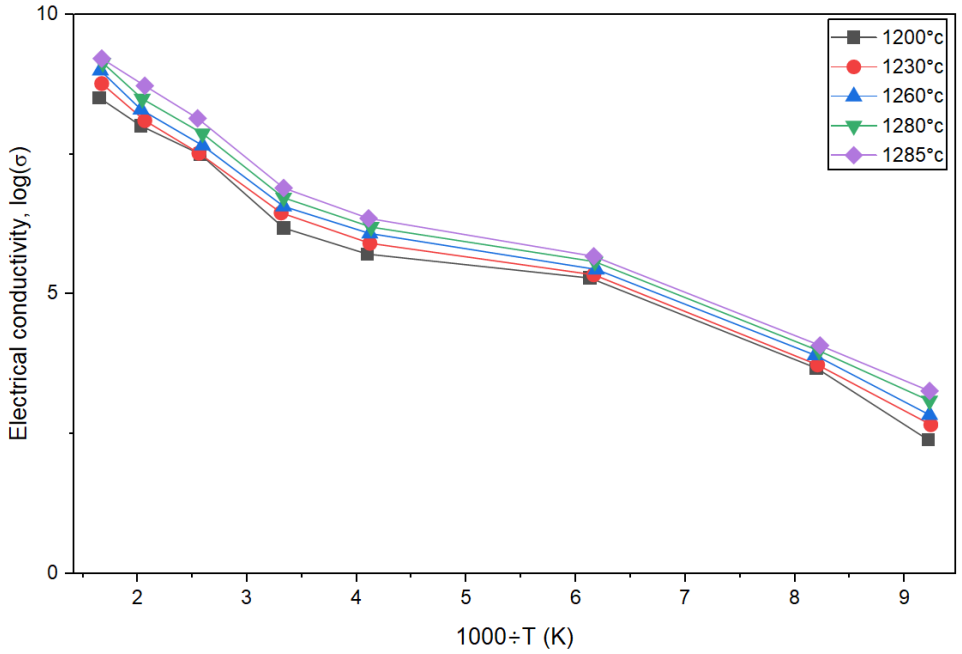

Figure 8: Sintering temperature on electronic conductivity and comparison with LSCM and LSGM

Density

The theoretical densities of the composites were estimated by the rule of mixtures. Bulk density was obtained via the Archimedes method, and relative density was computed as the ratio of bulk to theoretical density. Figures 9–10 depict the influence of ZrO_2 addition on density for pellets sintered at 1200 °C. As the ZrO_2 mole fraction on the A site increased from 0.05 to 0.20, the measured bulk density rose correspondingly, consistent with enhanced packing and pore filling by the fine ZrO_2 particles. Across the compositions examined, the calculated theoretical density ranged from ~4.55 to 4.85 g•cm^{-3}, with the highest value near x(ZrO_2) = 0.05 and the lowest near x = 0.02 (reported for completeness). For clarity, the theoretical density curves are plotted alongside the experimental bulk densities in Figures 3.3.1–3.3.2. Since the smaller Zr substitute the larger La in the perovskite structure so the theoretical density increased due to compactness of the composites with the continuous addition of ZrO_2. Similar result was also obtained by Jeong-Ho Kim 6.31gcm–3 for $La_{0.58}Sr_{0.4}Co_{0.2}Fe_{0.8}O_3$ (LSCF) [21].

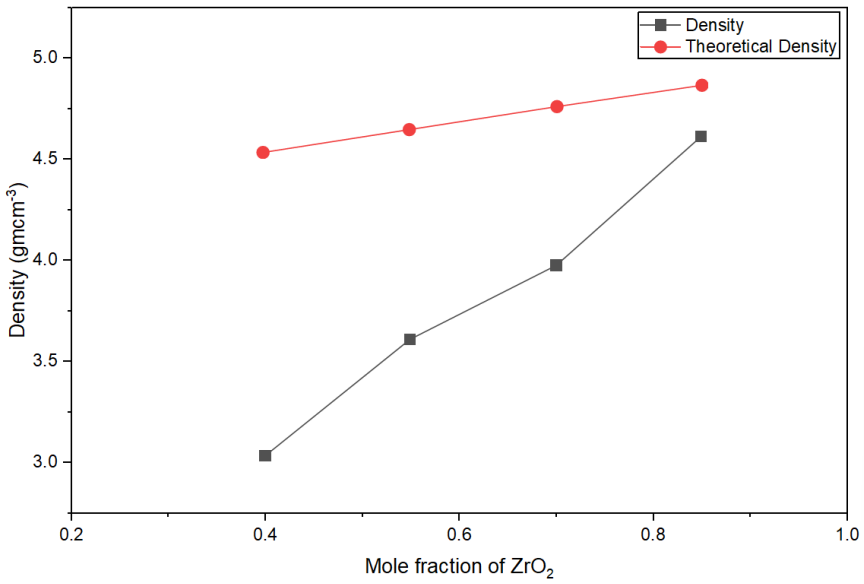

Figure 9: Effect of Addition of ZrO_2 Density of Perovskite

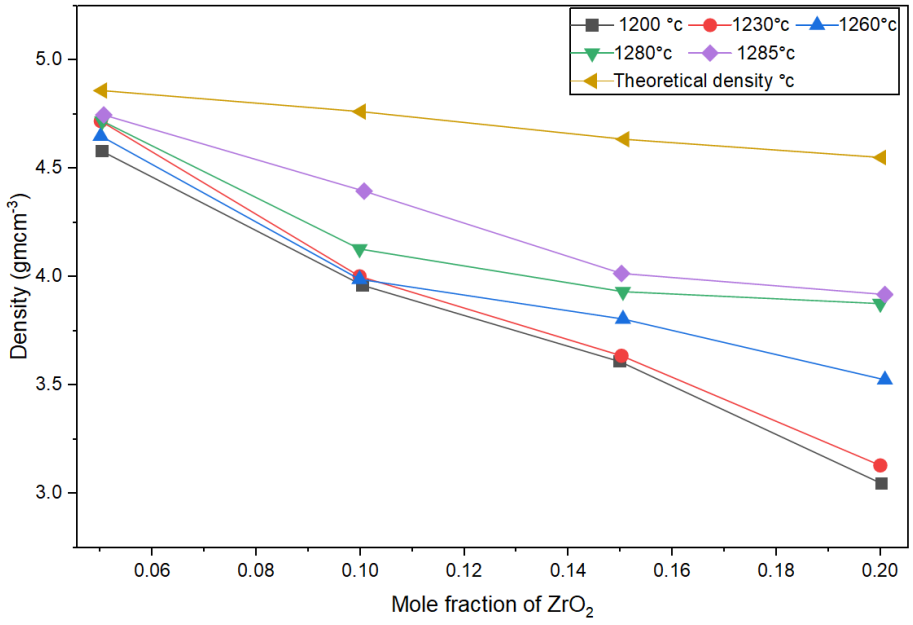

Figure 10: Sintering Temperature Density of Perovskite Structure

Hardness

Figure 11 summarizes the influence of ZrO_2 addition on the Vickers microhardness of the perovskite composites. With ZrO_2 substituting the A site cation and MnO2 occupying the B site. increasing the ZrO_2 mole fraction from 0.10 to 0.20 raises the hardness from ~84.5 HV to ~158 HV. At higher ZrO_2 contents, a decline in hardness is anticipated. Consistent with densification behavior, Vickers hardness correlates positively with bulk density and negatively with open porosity; the peak hardness occurs where density is maximized and porosity minimized. Acceptable hardness value of 0.70 ± 0.01 Gpa characterized by Nurul Akidah Baharuddin [22].

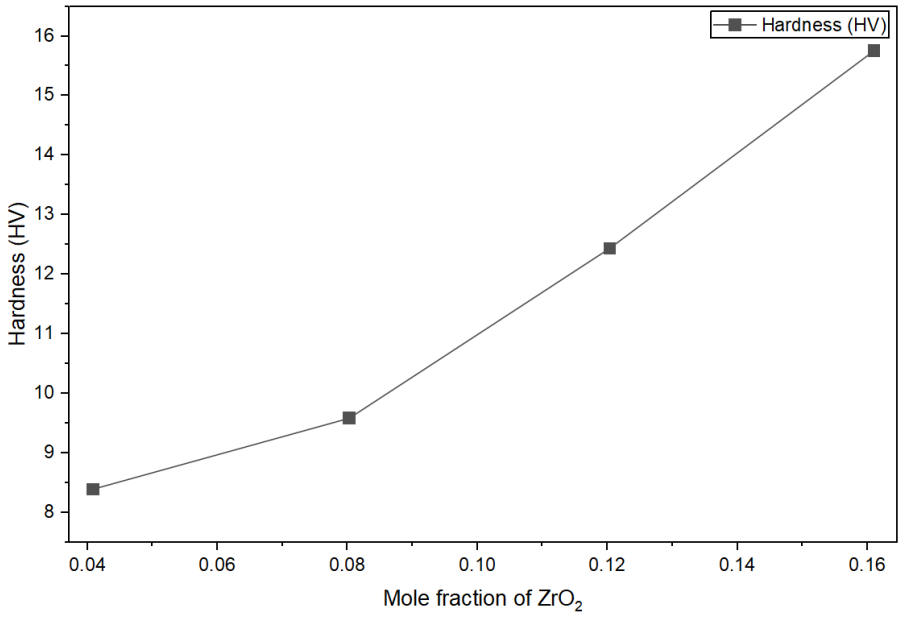

Figure 11: Hardness vs Sintering Temperature Graph

Porosity

Figure 12 and 13 shows the effect of addition of ZrO_2 on the porosity of the composites. The porosity was maximum 14.02 % at 0.05 mole fraction of ZrO_2 and decreased with the addition of substitution. The lowest porosity was not located until 0.20 mole fraction of the doping material. The porosity reduced due to the filling of voids in the composite by ZrO_2 nanoparticles as shown in figure 12 and 13. The further addition of ZrO_2 and MnO2 will increase the porosity. However, as amount of the doping material is increased additional internal defect will ensue. Ultimately the bigger grain expanded the inter-granular space that caused the enhancement of the porosity. Porosity showed an inverse relationship to density with ZrO_2 content: porosity reduced and density enhanced and the minimal porosity came with the composition with the supreme density. In the case of SOFC cathodes open porosity is typically desirable at around 40% or so. [23].

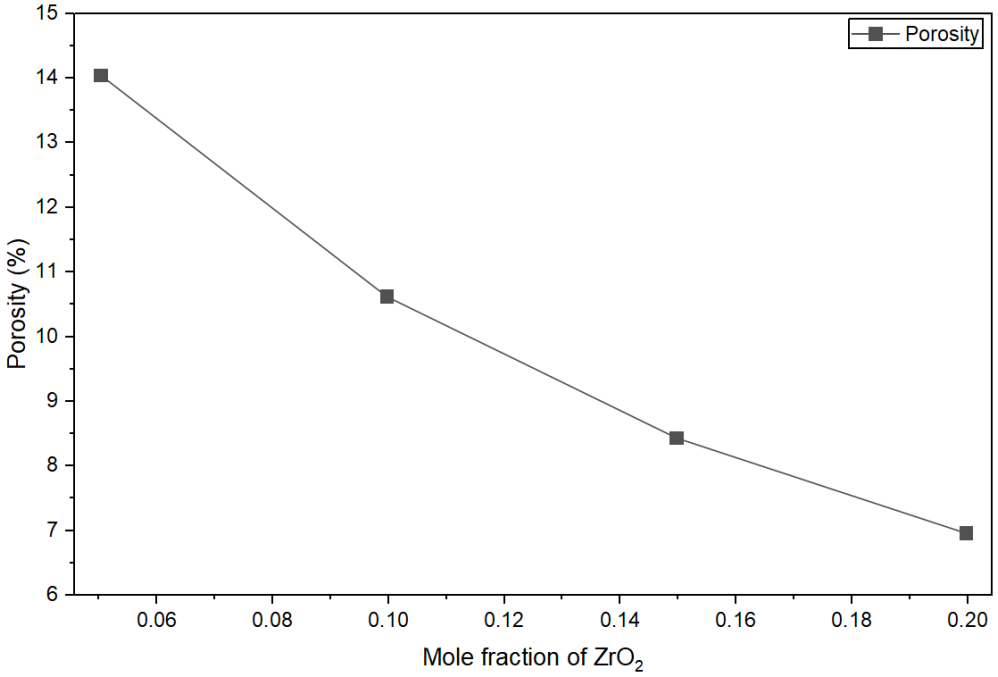

Figure 12: Effect of Addition of ZrO_2 on Porosity of Perovskite Structure

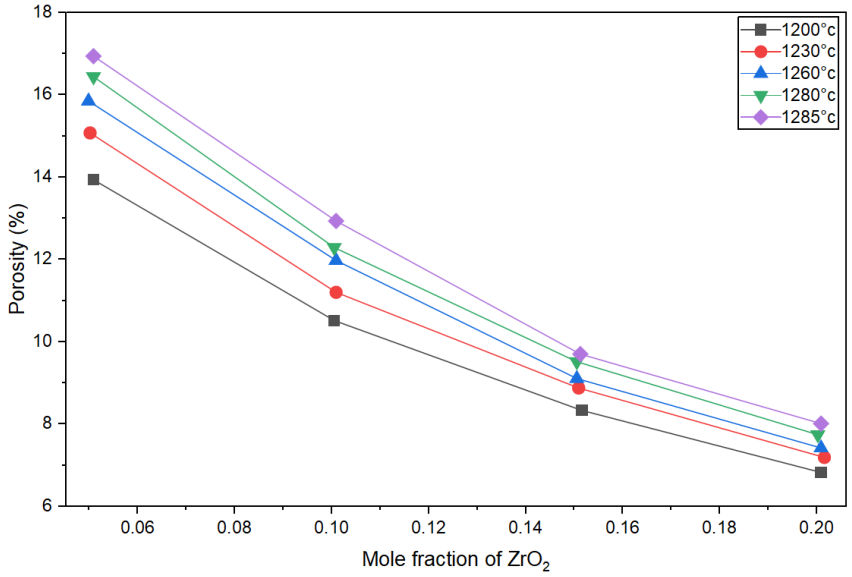

Figure 13: Sintering Temperature on Porosity of Perovskite Structure

Diametral Tensile Strength (DTS)

Figure 14 and 15 shows that with the increase of doping material of smaller size than the core material of perovskite structure, DTS was increased. It is because the smaller Zr replace the larger La and Mn replace the Co. From figure it was observed that the diametral tensile strength is increased from 16.5 (MPa) to 26 (MPa) as doping concentration increases from 0.1 to 0.20 mole fraction of ZrO2 and MnO2. Based on the above finding it was made clear that DTS was maintained at higher rates as the density was higher. Yet, as porosity went up, DTS was found to decrease. The differences between hardness and DTS and that of density and porosity of the composites are inverses. The critical point was not obtained up to doping material in the range of 0.20 mole fraction above which DTS would begin to worsen with the increase of inner damages to the structure. Camille Gazeau has already characterized DTS of several perovskites, which are given in table 3.1. The DTS of $La_{1-x}Zr_xCo_{1-y}MnyO_3$ is higher than LBFCo5573 and less than others [24]. This is because of the impact of the manufacturing process on the mechanical properties.

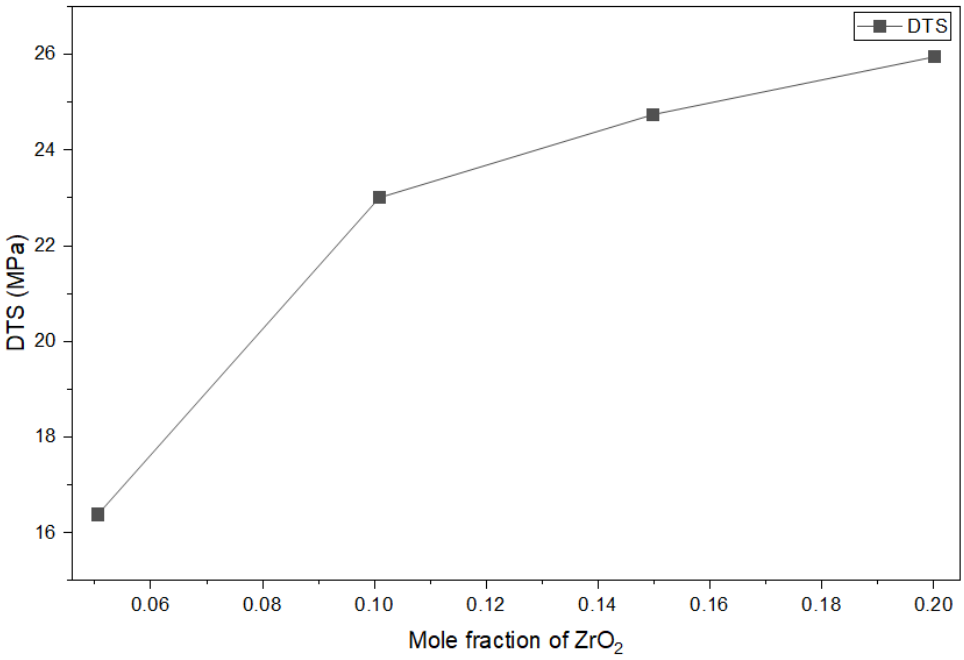

Figure 14: Effect of Addition of ZrO_2 on DTS of Perovskite Structure

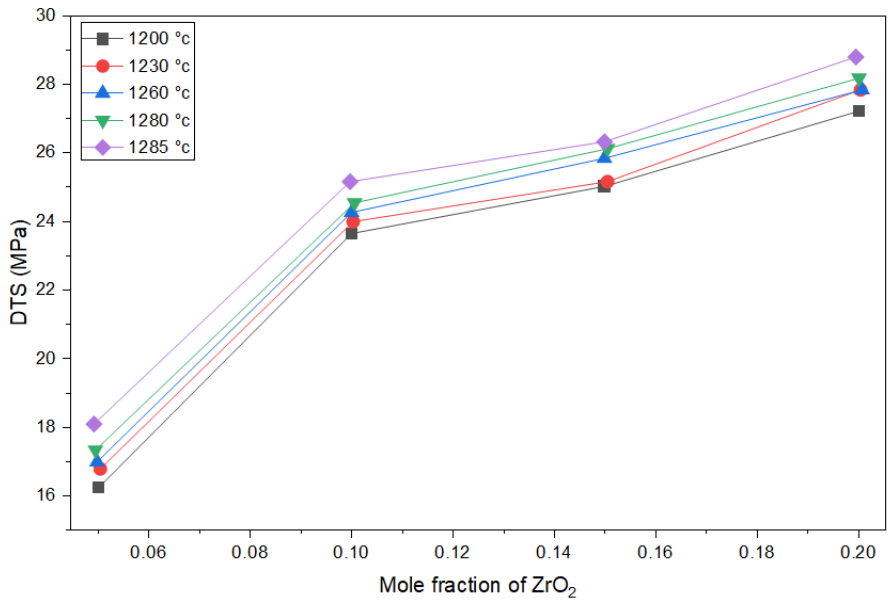

Figure 15: Sintering Temperature on DTS of Perovskite Structure

Name	DTS (MPa)
$La_{0.5}Ba_{0.5}Fe_{0.7}Co_{0.3}O_3$ (LBFCo5573)	18
$La_{0.2}Sr_{0.8}Fe_{0.7}Ga_{0.3}O_3$ (LSFG2873)	31
$La_{0.5}Sr_{0.5}Fe_{0.7}Ga_{0.3}O_3$ (LSFG5573)	46
$La_{0.5}Sr_{0.5}Fe_{0.3}Ga_{0.7}O_3$ (LSFG5537)	66
$La_{0.8}Sr_{0.2}Fe_{0.7}Ga_{0.3}O_3$ (LSFG8273)	76
$La_{0.9}Sr_{0.1}Fe_{0.7}Ga_{0.3}O_3$ (LSFG9173)	94

Table 3: Diametral Tensile Strength of Different Perovskite Material [24]

Compressive Strength (rectangular specimen)

As Figure 16 indicates, the compressive strength is enhanced by the increasing content of the dopant that has a smaller ionic size when compared to the host cation in perovskite. This can be explained by substituting smaller Zr by larger La and Co with larger Mn in a lattice. From figure it was observed that the compressive strength is increased from 59 (MPa) to 86 (MPa) as doping concentration increases from 0.1 to 0.20 mole fraction of ZrO_2 and MnO_2. The density was increased with an increase in compressive strength. But as porosity increased, compressive strength also decreased. The composites have the opposite of hardness and DTS to the density and porosity.

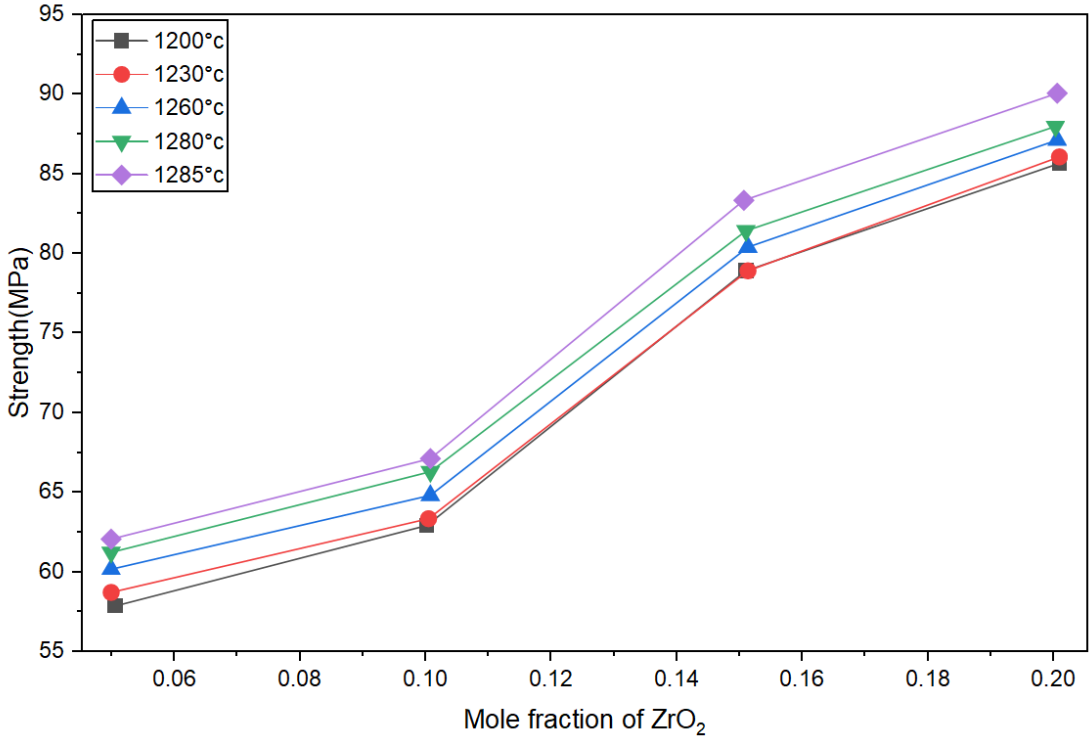

Figure 16: Sintering Temperature of Compressive Strength of Perovskite Structure

Conclusion

• Fabrication of wet type ball mill is done.

• New directions of further development of solid oxide fuel cells (SOFCs) were revealed. It also helped to demystify the existing system constraints as well as the system futures studied; most of them being focused on cathode materials. In the case of electrolytes, there are current directions trending towards the creation of intermediate-temperature solid- oxide fuel cells (IT-SOFCs) which, besides avoiding a temperature increase, attempt to (i) operate at lower temperature without reducing oxygen-ion conduction, (ii) decrease sintering temperature to facilitate manufacturing, and (iii) improve mechanical properties of hardness, fracture toughness, and flexural (bending) strength.

• By various literature studies, it was found that $LaCoO_3$ is serving most as cathode material because of its high electrical conductivity, low thermal expansion, high chemical and thermal stability. Various additives like La2O3, Co2O3, ZrO2 and MnO_2 etc. are being doped into LaCoO3 for improving performance.

• In this project and thesis, composite materials of LaCoO3 doped with different ZrO2 concentrations were fabricated via the solid-state reaction method. The concentrations of ZrO2 were 5 wt%, 10 wt%, 15 wt%, and 20 wt% and MnO2 kept 30wt%

• Testing on physical, mechanic and electrical characterization of fabricated composite from different batches were underway.

• Progressive incorporation of ZrO_2 (x = 0.05–0.20; A-site substitution with MnO_2 on the B site) led to systematic improvements in physical and mechanical performance—namely higher bulk density, reduced open porosity, increased Vickers hardness, and greater diametral tensile strength (DTS). The hardness rose from ~84.5 HV at x ≈ 0.10 to ~158 HV at x ≈ 0.20, while DTS increased from ~16.5 MPa to ~26 MPa across the same composition interval. These gains are consistent with enhanced densification and pore elimination induced by fine ZrO_2 additions.

• Sintering temperature effect was analyzed and results were investigated.

References

1. History of Ball Mill - Productivity.
2. Stambouli, A. B., & Traversa, E. (2002). Solid oxide fuel cells (SOFCs): a review of an environmentally clean and efficient source of energy. Renewable and sustainable energy reviews, 6(5), 433-455.
3. Stambouli, A. B., & Traversa, E. (2002). Solid oxide fuel cells (SOFCs): a review of an environmentally clean and efficient source of energy. Renewable and sustainable energy reviews, 6(5), 433-455.
4. Data from The International Fuel Cells, a United Technology Company. Fuel Cells Review. 2000.
5. Wet Ball Milling Vs Dry Ball Milling | Orbis Machinery, LLC.
6. Dusastre, V., & Kilner, J. A. (1999). Optimisation of composite cathodes for intermediate temperature SOFC applications. Solid state ionics, 126(1-2), 163-174.
7. Bharadwaj, S. R., S. Varma, and B. N. Wani. "Electroceramics for fuel cells, batteries and sensors." Functional Materials (2012): 639-674.
8. Calka, A., & Radlinski, A. P. (1991). Universal high-performance ball-milling device and its application for mechanical alloying. Materials Science and Engineering: A, 134, 1350-1353.
9. Lomakin, V., Khanin, S., Putivtseva, N., Zaitseva, T., & Pusnaya, O. (2018). METHOD OF SELECTING THE RATIONAL

STRUCTURE OF THE INTRA-MILL DEVICE WHILE DESIGNING A BALL MILL. Вісник Національної академії керівних кадрів культури і мистецтв, (3).
10. Tang, J., Zhao, L. J., Zhou, J. W., Yue, H., & Chai, T. Y. (2010). Experimental analysis of wet mill load based on vibration signals of laboratory-scale ball mill shell. Minerals Engineering, 23(9), 720-730.
11. Fuerstenau, D. W., & Abouzeid, A. Z. (2002). The energy efficiency of ball milling in comminution. International Journal of Mineral Processing, 67(1-4), 161-185.
12. Pladevall, B. S., de Aguirre, A., & Maseras, F. (2021). Understanding ball milling mechanochemical processes with DFT calculations and microkinetic modeling. ChemSusChem, 14(13), 2763-2768.
13. Li, L., Kong, Z., Yao, B., Yang, H., Gao, Z., Xu, L., ... & Lin, Z. (2020). An efficient and durable perovskite electrocatalyst for oxygen reduction in solid oxide fuel cells. Chemical Engineering Journal, 396, 125237.
14. Kim, J. H., & Manthiram, A. (2008). LnBaCo2O5+ δ oxides as cathodes for intermediate-temperature solid oxide fuel cells. Journal of the Electrochemical Society, 155(4), B385.
15. Zhou, Q., Wei, W. C. J., Guo, Y., & Jia, D. (2012). LaSrMnCoO5+ δ as cathode for intermediate-temperature solid oxide fuel cells. Electrochemistry communications, 19, 36-38.
16. Petric, A., Huang, P., & Tietz, F. (2000). Evaluation of La–Sr–Co–Fe–O perovskites for solid oxide fuel cells and gas separation membranes. Solid State Ionics, 135(1-4), 719-725.
17. Teraoka, Y., Nobunaga, T., Okamoto, K., Miura, N., & Yamazoe, N. (1991). Influence of constituent metal cations in substituted LaCoO3 on mixed conductivity and oxygen permeability. Solid State Ionics, 48(3-4), 207-212.
18. Stevenson, J. W., Armstrong, T. R., Carneim, R. D., Pederson, L. R., & Weber, W. J. (1996). Electrochemical Properties of Mixed Conducting Perovskites La1− x M xCo1− yFey O 3− δ (M= Sr, Ba, Ca). Journal of the Electrochemical Society, 143(9), 2722.
19. Huang, X., Pei, L., Liu, Z., Lu, Z., Sui, Y., Qian, Z., & Su, W. (2002). A study on PrMnO3-based perovskite oxides used in SOFC cathodes. Journal of alloys and compounds, 345(1-2), 265-270.
20. Kumar, A., Sivaprahsam, D., & Thakur, A. D. (2018). Improvement of thermoelectric properties of lanthanum cobaltate by Sr and Mn co-substitution. Journal of Alloys and Compounds, 735, 1787-1791.
21. Li, N., Verma, A., Singh, P., & Kim, J. H. (2013). Characterization of La0. 58Sr0. 4Co0. 2Fe0. 8O3− δ–Ce0. 8Gd0. 2O2 composite cathode for intermediate temperature solid oxide fuel cells. Ceramics International, 39(1), 529-538.
22. Baharuddin, N. A., Aman, N. A. M. N., Muchtar, A., Somalu, M. R., Samat, A. A., & Aznam, M. I. (2019). Structural, morphological, and electrochemical behavior of titanium-doped SrFe1-xTixO3-δ (x= 0.1–0.5) perovskite as a cobalt-free solid oxide fuel cell cathode. Ceramics International, 45(10), 12903-12909.
23. Ghosh, A., Sahu, A. K., Gulnar, A. K., & Suri, A. K. (2005). Synthesis and characterization of lanthanum strontium manganite. Scripta Materialia, 52(12), 1305-1309.
24. Gazeau, C., Gillibert, J., Blond, E., Geffroy, P. M., & Richet, N. (2015). Experimental set up for the mechanical characterization of plane ITM membrane at high temperature. Journal of the European Ceramic Society, 35(14), 3853-3861.